Journal of Power Sources 195 (2010) 5564–5572

Contents lists available at ScienceDirect

Journal of Power Sources

journal homepage: www.elsevier.com/locate/jpowsour

Controlled synthesis of carbon-supported Pt_3Sn by impregnation-reduction and performance on the electrooxidation of CO and ethanol

S. García-Rodríguez, M.A. Peña, J.L.G. Fierro, S. Rojas*

Grupo Energía y Química Sostenibles, Instituto de Catálisis y Petroleoquímica, CSIC, C/Marie Curie 2, E-28049 Madrid, Spain

ARTICLE INFO

Article history:
Received 5 November 2009
Received in revised form 25 February 2010
Accepted 6 March 2010
Available online 16 March 2010

Keywords:
Impregnation
Pt_3Sn
Ethanol
Thermal analysis
EDS

ABSTRACT

The paper discusses experimental features relevant to the synthesis of carbon-supported Pt_3Sn nanosized particles by impregnation-reduction of the salt precursors in carbon. Colloidal techniques are proposed as the most suitable ones for obtaining carbon-supported nanosized Pt_3Sn particles. In most cases, the electrocatalysts obtained have a wide range of Pt and Sn phases, including bimetallic ones. The synthesis of similar materials by impregnating readily available precursors such as $SnCl_2$ and H_2PtCl_6 yields Pt-enriched catalyst precursors. In order to obtain electrocatalysts with the desired Pt:Sn = 3 atomic stoichiometry, it is necessary to eliminate chloride ions prior to thermal treatments. Microscopy characterization and thermal stability studies of the fresh and treated bimetallic materials reveal that if such ions are present, Sn is eliminated as volatile $SnCl_x$ species at around 120–130 °C. Chloride elimination is achieved by ageing the catalyst precursor in water to ensure the complete hydrolysis of the $SnCl_2$ precursor. This treatment should be performed once $SnCl_2$ has been deposited on the carbon to avoid the formation of large Sn-oxide aggregates. A further thermal treatment in hydrogen results in the formation of the desired Pt_3Sn intermetallic phase. The performance of the Pt_3Sn/C samples in the CO and ethanol electrooxidation reaction has been studied by means of electrochemical techniques. The electrocatalysts prepared by the impregnation-reduction approach match the performance of the state-of-the-art Pt_3Sn samples prepared by colloidal techniques.

1. Introduction

Direct alcohol fuel cells (DAFC) are devices that extract the chemical energy accumulated in molecules such as methanol or ethanol producing a potential difference which results in electrical work [1]. Ethanol has a number of advantages over methanol; it can be produced in a sustainable way, easily stored and transported and is less harmful or corrosive than methanol. The complete oxidation of ethanol releases 12 electrons per molecule; its standard electromotive force E^0_{Eq} = 1.145 V, being similar to that of methanol [2]. However, a number of issues, particularly those related to the performance of the electrocatalyst, should be improved in order to implement direct ethanol fuel cell technology.

An efficient ethanol electrooxidation catalyst should combine at least two features: (i) high tolerance to CO and other intermediate species generated over the surface of the electrocatalyst during alcohol electrooxidation; and (ii) ability to break the C–C bond of the ethanol molecule under mild conditions. Pt modification with more oxophilic metals such as Ru [3], Mo [4] or Sn [5] is the best way of improving CO tolerance. This is because such oxophilic atoms promote the formation of OH_{ad} species (involved in the CO_{ad} oxidation reaction) at potentials that are more negative than on monometallic Pt. Among those, Sn-modified Pt electrocatalysts are the most active formulations [6–9]. There is also widespread consensus that the Pt_3Sn phase is the most active one in the CO and early stages of the ethanol electrooxidation process [6,10,11]. Ethanol electrooxidation on Pt_3Sn/C results in partial oxidation products, mainly acetic acid and acetaldehyde [12]. $PtRhSnO_2$ ternary electrocatalysts capable of oxidizing ethanol to CO_2 have recently been reported [13–15].

Although the impregnation-reduction method has been frequently used for the synthesis of PtSn supported on inorganic carriers such as SiO_2 or Al_2O_3 or SAPO, this approach has rarely been employed for the synthesis of carbon-supported electrocatalysts [16–19]. In general, the metal content in those samples is ca. 1–2 wt%, well below the demands of a state-of-the-art fuel cell electrocatalyst. A number of routes have been explored for the synthesis of carbon-supported bimetallic PtSn samples. In general, they lead to materials composed of a wide range of phases, such as metallic and/or oxide Pt, Sn oxides or PtSn solid solutions of different stoichiometry. Lamy et al. stated that the Bönnemann method renders the most active electrocatalysts, allowing some control of the different metallic phases [20,21]. The microemulsion method [20] and especially the polyol method [22] have been

* Corresponding author. Tel.: +34 91 585 4863; fax: +34 91 585 4760.
E-mail address: srojas@icp.csic.es (S. Rojas).

0378-7753/$ – see front matter © 2010 Elsevier B.V. All rights reserved.
doi:10.1016/j.jpowsour.2010.03.026

proposed as the most suitable approaches for synthesizing nanosized carbon-supported bimetallic PtSn samples. The latter method affords Sn species in multivalence states [23,24] that, according to some reports, could be beneficial for the final activity of the catalysts [25]. Nevertheless, the exclusive formation by the polyol method of alloyed PtSn phases, along with a variable amount of SnO_2, is also reported [26]. These methods yield only partially alloyed particles due to the lack of thermal treatments imposed by the use of low boiling point solvents. A high-temperature colloidal approach has recently been proposed for the synthesis of Pt_3Sn nanoparticles [27]. Other approaches focus on the modification of the surface of carbon-supported Pt particles with Sn-organic precursor. In general, these routes lead to the exclusive formation of Pt_3Sn [6,28,29]. Hydrothermal treatment [30] and the Pechini-Adams method [31] have recently been proposed for the synthesis of carbon-supported PtSn bimetallics, which yield samples of a composition similar to those reported by other methods. An interesting approach to fix the Pt to the Sn atomic stoichiometry of the samples is the use of Pt–Sn complexes as metallic precursors [32,33]. Finally, and regardless of the synthesis method, obtaining the most desired Pt_3Sn phase requires thermal treatment in a reducing atmosphere.

Whichever the synthesis route and the electrocatalytic performance, a certain lack of consistency between different electrocatalysts has been pointed out [32], suggesting the coexistence of a number of metal and/or oxidized phases in those systems. On the other hand, most reports fail to give the actual metallic loading of the final catalysts, or the Pt to Sn stoichiometry of the particles, or, more importantly for the sake of reproducibility of the methods, the target metal loading and Pt:Sn atomic ratio.

This paper describes the synthesis of carbon-supported bimetallic PtSn samples by impregnation. The progress of the synthesis is followed by a number of characterization techniques such as electron microscopy, energy dispersive X-ray spectroscopy (EDS), X-ray diffraction and thermogravimetric analysis. The precise reaction conditions under which the Pt_3Sn/C is formed and under which Sn losses were observed are discussed. The performance of the different PtSn/C samples in the CO and ethanol electrooxidation reactions was evaluated by electrochemical methods.

2. Experimental

2.1. Synthesis of PtSn/C

The following chemicals have been used for the synthesis of the samples; H_2PtCl_6 (Johnson Matthey), $SnCl_2$ anhydrous (Alfa Aesar), Vulcan XC-72R (Cabot) and HCl (PRS-Codex from Panreac). Pt/C (40 wt%) (Johnson Matthey) was used as reference catalyst. Type II water (Ellix 10, Millipore) is used unless otherwise stated. The target composition for the carbon-supported PtSn bimetallic samples is 40 wt% metal base and Pt:Sn 3:1 atomic ratio. Two samples with a 30 and 20 wt% metal base and Pt:Sn 3:1 atomic ratio were also prepared. Table 1 summarizes the main synthesis details and nomenclature of the samples.

2.1.1. Synthesis of carbon-supported PtSn

The appropriate amounts of H_2PtCl_6 and $SnCl_2$ for obtaining a Pt_{at}:Sn_{at} = 3 were dissolved in water and 3 M HCl, respectively, added to a dispersion of carbon (to obtain a solid with a 40 wt% metal loading) in 3 M HCl and stirred for 1 h. A electrocatalyst precursor, labeled as PtSn-*fresh*, was recovered by solvent evaporation at reduced pressure at 70 °C. At this point, two different routes were followed. In the first approach, aliquots of PtSn-*fresh* were subjected to different thermal treatments: (i), under flowing H_2/He (10 vol% H_2) at 250 °C for 2 h at a heating rate of 10 °C min^{-1} (labeled as PtSn-*red*); (ii) under static air at 250 °C for 2 h followed by a thermal treatment under flowing H_2/He (10 vol%) for 2 h at a heating rate of 10 °C min^{-1} (labeled as PtSn-*calred*); (iii) under static air at 250 °C for 2 h (labeled PtSn-*cal*). In the second approach, an aliquot of PtSn-*fresh* was dispersed in water under stirring and a electrocatalyst precursor was recovered by filtration. During this treatment, the recovered mother liquor turned pale yellow. The sample, recovered by filtration, was dried at 70 °C and treated under static air at 250 °C for 2 h (labeled as PtSn-*rincal*). Finally, a further aliquot of PtSn-*fresh* was subjected to a series of dispersion in water followed by evaporations in a rotary evaporator steps until the pH of the recovered water was ca. 6.5. The electrocatalyst obtained after water evaporation was dried and labeled as PtSn-*aged*. This sample was subjected to thermal treatment under static air at 250 °C for 2 h followed by a thermal treatment at 250 °C under flowing H_2/He (10 vol%) for 2 h at a heating rate of 10 °C min^{-1} (labeled as PtSn-*agedcalred*).

In order to prove reproducibility of the impregnation-reduction method, two further Pt_3Sn/C electrocatalysts with metal loadings of 30 and 20 wt% were prepared. The protocol for the synthesis is identical to that described above for PtSn-*agedcalred*. First, the appropriate amounts H_2PtCl_6 and $SnCl_2$ for obtaining a Pt_{at}:Sn_{at} = 3 were dissolved in water and 3 M HCl, respectively, added to a dispersion of carbon (to obtain two catalysts with a 30 and 20 wt% metal loading) in 3 M HCl and stirred for 1 h. A electrocatalyst precursor was recovered by filtration and washed with abundant water in a rotary evaporator until the pH of the recovered water was ca. 6.5. The sample was subjected to two consecutive thermal treatments first under static air at 250 °C for 2 h and then at 250 °C under flowing H_2/He (10 vol%) for 2 h at a heating rate of 10 °C min^{-1}. The obtained electrocatalysts were labeled as 30-PtSn-*agedcalred* and 20-PtSn-*agedcalred*.

The nomenclature and most relevant preparation details of all samples are collected in Table 1.

2.1.2. Reference samples for thermal analysis

The Pt/C, Pt_3Sn_1/C and Pt_1Sn_3/C samples were prepared by adding a water solution of the appropriate concentration of the metal precursors to a dispersion of carbon in water for thermal analysis purposes. Samples were recovered by removal of water in a rotary evaporator and subjected to thermal analysis without prior treatment.

2.2. Physicochemical characterization

An Extra-II TXRF spectrometer (Rich & Seifert) was used to estimate the metal loading of the samples. X-ray diffraction (XRD) analysis was performed using an X-ray diffractometer from X'Pert Pro PANalytical. Bragg's angles (2θ) between 2° and 90° were recorded at a rate of 0.04° per step and a count time of 20 s per step. Selected 2θ angle regions were recorded for 500 s in order to magnify the intensity of the desired reflections by enhancing the signal-to-noise ratio. The assignment of the diffraction lines to the corresponding crystalline phases was carried out by comparison with Powder Diffraction Files (PDF) from the International Centre for Diffraction Data (ICDD) (a.k.a.) Joint Committee on Power Diffraction Standards (JCPDS).

Transmission electron microscope (TEM) images were recorded in a JEOL microscope model JEM-2100F. Specimens for analysis were dispersed in ethanol in an ultrasonic bath and a few drops were deposited over a 200 mesh copper lacy carbon grid from SPI. EDS analysis was performed in an Oxford INCAx-Sight EDS detector using an INCA Energy software package.

Table 1
Nomenclature, composition and most relevant synthetic details of the samples.

Sample	Metal content (at%)[a]		Precursor	Treatment[b]
	Pt	Sn		
PtSn-*fresh*	75	25	Metal salts	
PtSn-*red*	~97	~3	PtSn-*fresh*	l. H_2/He 25–250 °C
PtSn-*calred*	~97	~3	PtSn-*fresh*	1. Air; 250 °C; 2 h 2. H_2/He, 25–250 °C
PtSn-cal	~90	~10	PtSn-*fresh*	1. Air; 250 °C; 2 h
PtSn-*rincal*	50	50	PtSn-*fresh*	1. Washed with water 2. Air; 250 °C; 2 h
PtSn-*aged*	75	25	PtSn-*fresh*	1. Washed till pH ~6.5
PtSn-*agedcalred*	75	25	PtSn-*aged*	1. Air; 250 °C; 2 h 2. H_2/He; 25–250 °C
30-PtSn-*agedcalred*	75	25	Metal salts	1. Washed till pH ~6.5 2. Air; 250 °C; 2 h 3. H_2/He; 25–250 °C
20-PtSn-*agedcalred*	75	25	Metal salts	1. Washed till pH ~6.5 2. Air; 250 °C; 2 h 3. H_2/He; 25–250 °C

[a] Atomic content referred only to Pt and Sn.
[b] Further preparation details are reported in Section 2.1.1.

Thermogravimetric analysis (TGA) under controlled atmosphere was carried out on a Mettler Toledo TGA/SDTA851e, using 200 cm^3 min^{-1} of N_2 as carrier gas, 20 cm^3 min^{-1} of oxygen as reactive gas, and a heating rate of 10 °C min^{-1}.

Electrochemical studies were carried out at 25 °C in a thermostatic conventional three-compartment electrochemical glass cell. A glassy carbon rotating disk electrode (0.283 cm^2, GC-Typ zu628) was used as a substrate for the catalyst. Unless otherwise stated, current densities are referred to the geometric area of the electrode. Prior to each test, the electrode was polished with alumina 0.05 μm to obtain a mirror finish and rinsed with triply distilled water in an ultrasonic bath. An Ag/AgCl 3 M KCl electrode and a platinum wire were used as the reference and counter electrodes, respectively. All potentials are referred to the reversible hydrogen electrode (RHE). The samples under study were deposited onto the working electrode by means of an ink. To prepare the ink, 5 mg of the electrocatalyst, 30 μL of 5 wt% of Nafion solution (Aldrich), and 700 μL of Mili-Q water were dispersed in an ultrasonic bath for 45 min. 20 μL of the ink were dropped onto the electrode and dried at room temperature resulting in a uniform coating. A 0.1 M $HClO_4$ solution (Merck) was used as the electrolyte. All solutions were prepared with Mili-Q water. Electrochemical measurements were taken with a computer-controlled potentiostat/galvanostat EG&G 273A.

3. Results

3.1. Physicochemical characterization

The characterization data of sample PtSn-*fresh* reveal that it consists of an amorphous deposit of a material containing Pt and Sn on carbon. The atomic composition of the sample as determined from EDS analysis is Pt 75 wt%, Sn 25 wt% (unless otherwise stated, EDS analyses are referred to metal basis alone). The Pt/Sn atomic ratio equals 3, in good agreement with the nominal value. The PtSn-*fresh* diffractogram (not shown) shows only broad diffraction lines ascribed to the carbon support. Fig. 1 displays a micrograph of the PtSn-*fresh* sample showing amorphous particles on carbon. A number of Pt nanoparticles of around 1 nm size are observed.

When preparing supported catalysts, a calcination process is usually used to remove unwanted ions such as chloride or nitrate remaining from the metal precursors. Furthermore, the formation of the Pt_3Sn requires a thermal treatment in hydrogen at least at 200 °C [34]. However, it is also well known that particle agglomeration is favored during thermal treatments. It would therefore be expedient to avoid thermal treatments insofar as possible during synthesis. Hence, as a first approach, PtSn-*fresh* was treated under hydrogen flow without a previous calcination treatment, yielding the PtSn-*red* sample. This sample consists of well-dispersed nanoparticles (mean particle size of 4.0 ± 0.1 nm as deduced by counting more than 700 particles) deposited on carbon, as depicted in Fig. 2a. Unexpectedly, the amount of Sn in sample PtSn-*red* as deduced from EDS analyses of different areas (see Fig. 3) ranges between 2 and 4 at%, a value well below the nominal one. It should be noted that the parent sample had a Pt:Sn atomic content of 3 (see characterization data of PtSn-*fresh*).

Fig. 2b depicts a representative TEM image of PtSn-*calred*. This sample has been prepared by treating PtSn-*fresh* in static air and hydrogen (see further data in Section 2.1.1). The micrograph reveals the presence of well-dispersed particles of a mean size of 5.1 ± 0.2 nm. Again, the Pt:Sn atomic ratio deduced from the EDS analysis (Fig. 3) was much higher than expected, see Table 1. Furthermore, Cl was not found in either the PtSn-*red* or the PtSn-*calred* samples.

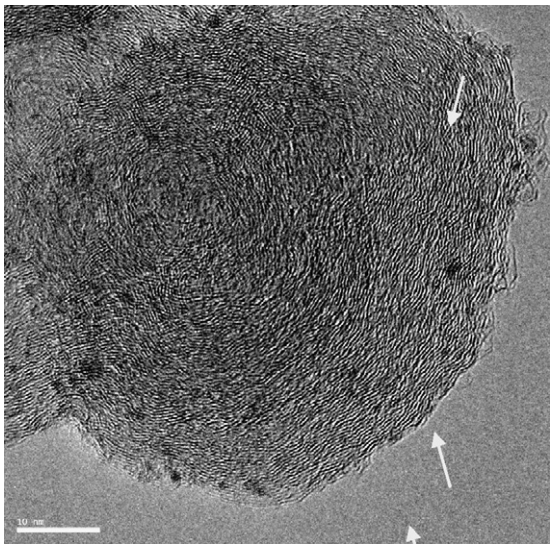

Fig. 1. Selected TEM image of PtSn-*fresh* showing the amorphous deposits (white arrows) of Pt and Sn.

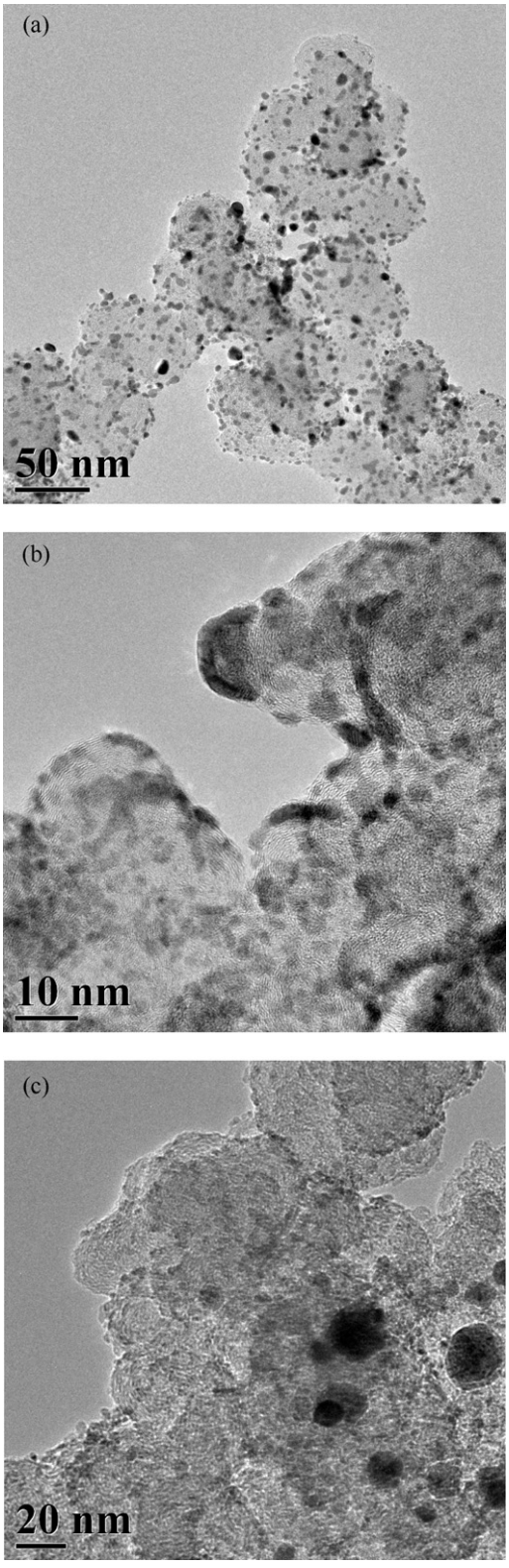

Fig. 2. Representative TEM images of PtSn-*red* (a), PtSn-*calred* (b), and PtSn-*rincal* (c) samples.

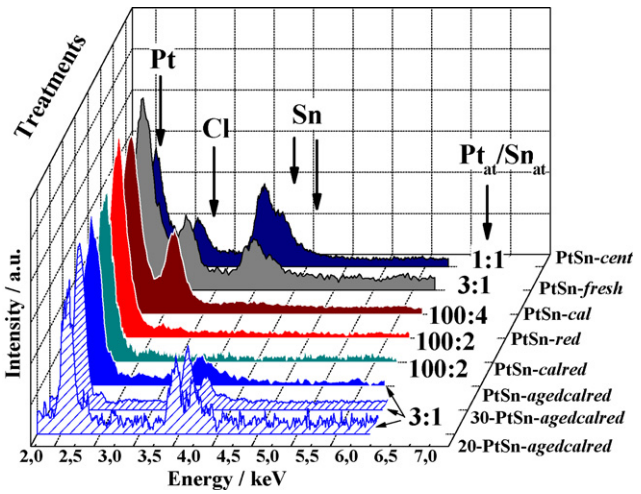

Fig. 3. Evolution of the Pt and Sn content with the synthesis route as determined by EDS analysis.

Similar results have been found for the PtSn-*cal* sample. EDS analysis (see Fig. 3) reveals that Pt is the predominant element, although energy lines of Sn and Cl are clearly observed in the spectrum. In this sample, the amount of Sn ranged between 8 and 12 at% (depending on the region analyzed), a value below the nominal one (25 at%). The Pt and Sn atomic contents found by EDS analysis of the PtSn/C samples are collected in Table 1.

Finally, characterization data of the PtSn-*rincal* sample reveal that it consists of well-dispersed nanosized particles along with large aggregates (see micrograph depicted in Fig. 2c) containing Pt, Sn and Cl, as revealed by the EDS analysis shown in Fig. 3. Noticeably, the Sn content of this sample, ca. 50 at%, is the highest in the series, doubling that of the parent sample (PtSn-*fresh*). This is because Pt is lost during synthesis, whereas Sn remains in the electrocatalyst, and in turn it indicates the need to treat PtSn-*fresh* in water before subjecting it to any thermal treatment to avoid Sn losses.

Sample PtSn-*aged* was characterized by EDS, XRD and microscopy analyses. Unlike the samples described above, the composition of this sample fulfils the nominal stoichiometry, that is, 3–1 at%, respectively, for Pt and Sn (see Table 1). A further analysis of this sample reveals that Pt and Sn are present as two isolated phases. Fig. 4a depicts a micrograph of the sample that indicates the presence of individual SnO_2 and Pt particles. The Fast Fourier Transform (FFT) image of the SnO_2 particle is shown in Fig. 4b. The inset to Fig. 4b is the simulated electron diffraction diagram of the area corresponding to SnO_2 particles aligned along the [0 0 1] zone axis. In this sample, Pt^0 particles are also detected by TEM. Fig. 4c is the FFT image of the Pt particle shown in Fig. 4a. The simulated electron diffraction diagram of the area corresponding to Pt particles aligned along the [1 1 0] zone axis is shown in the inset to Fig. 4c. Two features should be highlighted. On the one hand, Pt and Sn coexist as separate phases, with no solid solutions of either element being detected. On the other hand, although no reducing agents were added, Pt^0 particles are detected. It has been previously observed that certain carbon sites reduce Pt^{4+} and Pt^{2+} species to primary Pt^0 particles of ca. 1 nm, such as those observed in PtSn-*fresh* and PtSn-*aged* [35].

After subjecting PtSn-*aged* to two consecutive thermal treatments in static air and hydrogen, respectively, sample PtSn-*agedcalred* was obtained. EDS analysis reveals that the Pt:Sn atomic ratio = 3 is maintained even after thermal treatments. The X-ray diffraction pattern of the sample displayed in Fig. 5a shows the characteristic peaks of the Pt fcc phase. A certain broadening of the peaks to the lower 2θ values is also observed, indicating the presence of the Pt_3Sn phase. No peaks ascribed to SnO_2 or other isolated Sn phases are observed. As deduced from the micrograph in Fig. 5b, a good dispersion of the metal phase on carbon is also achieved, with the mean particle size being 3.6 ± 0.1 nm. Fig. 5c is a HRTEM

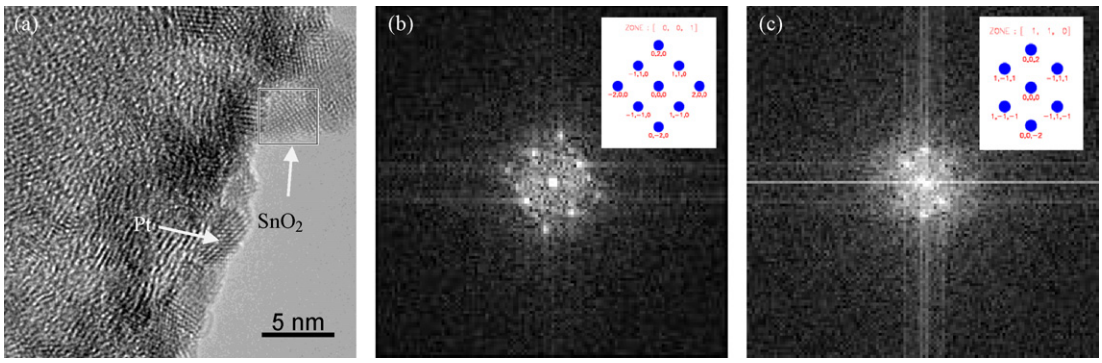

Fig. 4. (a) TEM image of PtSn-*aged* sample. The presence of SnO_2 and Pt is arrowed; (b) FFT image and simulated electron diffraction diagram in the [0 0 1] zone axis (inset) of the SnO_2 particle arrowed in (a); (c) FFT image and simulated electron diffraction diagram close to the [1 1 0] zone axis (inset) of the Pt particle arrowed in (a).

micrograph of sample PtSn-*agedcalred*, showing a faceted termination of the particles. The particle has an orientation close to the [1 1 0] zone axis. The intense 1 1 1 reflection from the Pt_3Sn alloy phase is observed, showing a spacing $d_{(1\,1\,1)}$ = 2.304 Å and a weak 0 0 2 reflection showing a spacing $d_{(0\,0\,2)}$ = 2.014 Å. This result, along with the XRD data, confirms the formation of the intermetallic Pt_3Sn phase. TXRF data confirm that the metal loading of the sample is ca. 39.2 wt%.

By taking into account the characterization results described thus far, it appears that subjecting the PtSn-*fresh* sample to thermal treatments, either in air hydrogen or air, results in severe Sn losses. On the other hand, Pt losses are recorded when rinsing the sample

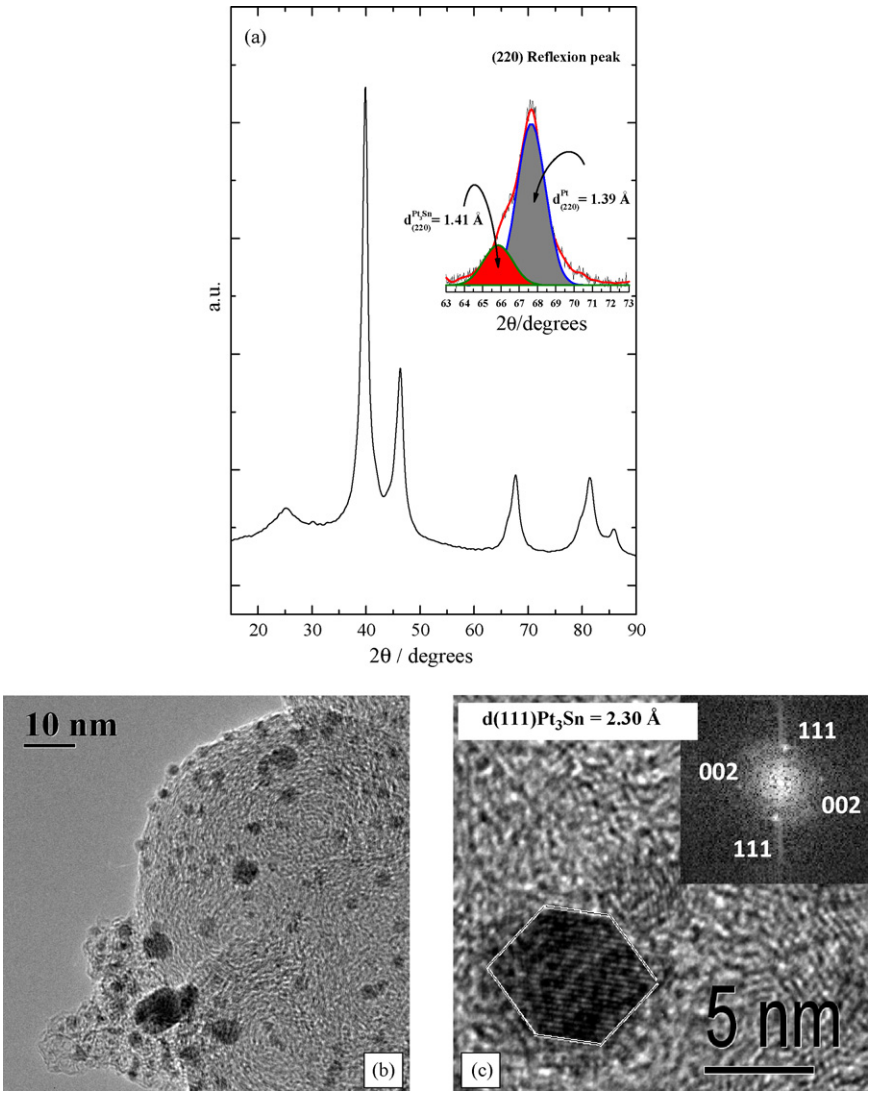

Fig. 5. (a) XRD profile of the sample PtSn-*agedcalred*, the inset is a magnification of the (2 2 0) diffraction peak highlighting the presence of two crystalline phases, with *a* (2 2 0) interplanar spacing *d* = 1.41 Å and 1.39 Å corresponding to the Pt_3Sn (PDF #35-1360) and Pt fcc (PDF #4-0802); (b) representative TEM image of the sample; (c) HRTEM image showing a preferential facet termination of individual particles. The inset is the FFT of the particle.

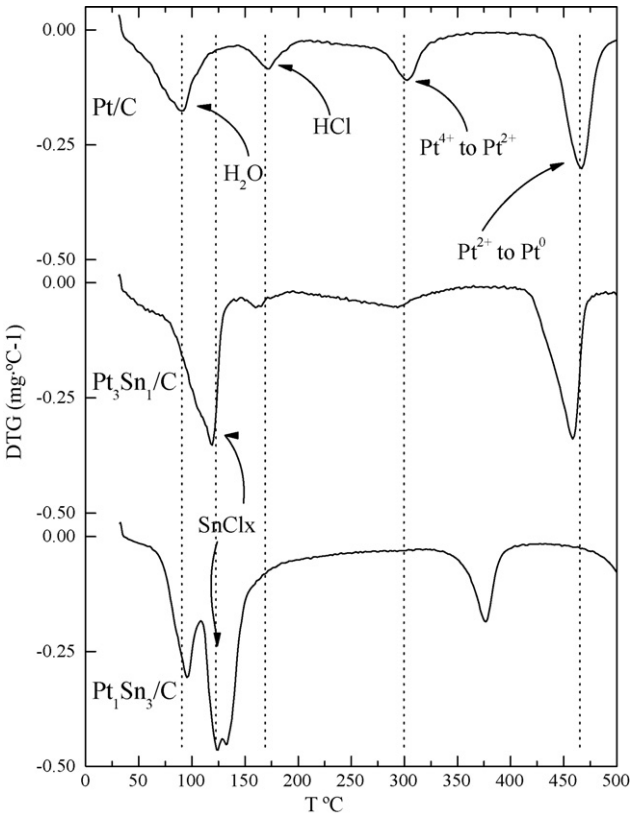

Fig. 6. Derivative thermogravimetric profile of the carbon-supported PtSn samples with increasing content of Sn recorded in air.

prior to thermal treatment, but Sn remains in the sample. In order to maintain Pt and Sn content at the nominal value, it is necessary to rinse the sample until the pH value of the obtained water is ≈7. This is because chloride ions are eliminated during this first treatment and Sn hydroxyl species are formed during the ageing step prior to thermal treatment. The effect of ageing in the synthesis of PtSn samples has been previously hinted by Lamy et al. [20].

3.2. Thermal stability of PtSn/C

To understand how Sn and Pt remain or not during the synthesis of PtSn samples, thermogravimetric analyses were conducted of Pt/C and Pt_3Sn_1/C and Pt_1Sn_3/C samples (see Section 2.1.2) in different atmospheres. The derivative of the TGA curve (DTG) recorded in air is depicted in Fig. 6. The DTG curve of Pt/C shows weight losses at 92, 170, 300 and 465 °C. The former one, at $T < 100$ °C is due to water removal. In line with previous studies [36], the peaks at ca. 170, 300 and 465 °C are ascribed, respectively, to HCl removal, Pt^{4+} to Pt^{2+} reduction and Pt^{2+} to Pt^0 reduction processes. Similar weight losses are observed for the PtSn samples; however, certain important differences should be noted. The DTG profile recorded for the Pt_3Sn_1/C sample displays the peak associated with the Pt^{2+} to Pt^0 reduction processes at 460 °C; the same temperature as that recorded for Pt/C. It also records a peak at ca. 300 °C (Pt^{4+} to Pt^{2+} reduction), but its intensity is much lower than that of the peak recorded for Pt/C. The peak ascribed to HCl removal appears at ca. 160 °C, although its intensity is much lower than that recorded for Pt/C. Remarkably, a further peak at ca. 120 °C appears. The DTG profile of the Pt_1Sn_3/C sample records no peaks between 160 and 170 °C; however, the intensity of the peak at ca. 120–130 °C increases noticeably as compared to that for Pt_3Sn_1/C. Weight losses recorded up to 200 °C are 30, 16 and 14 wt%, respectively, for Pt_1Sn_3/C, Pt_3Sn_1/C and Pt/C, that is, they become higher as the Sn content in the samples increases. A plausible scenario to explain the DTG profiles would involve assigning the peak between 120 and 130 °C to the loss of Sn and chloride ions, more likely as $SnCl_x$ species. Such assignment explains the decreasing intensity of the peak associated with HCl loss in the Sn-containing samples. The peak associated with such processes appears at ca. 170 °C in Pt/C, but it is hardly visible in Pt_3Sn/C and it is not observed in $PtSn_3$/C, as chloride ions are previously eliminated along with Sn at ca. 120–130 °C. Studies dealing with thermal decomposition of tin halides are scarce. Čerič et al. report that $SnCl_2$ melts at 217 °C and the initial temperature of the $SnCl_2$ decomposition process in Ar starts at 354 °C; however, when heating $SnCl_2$ in air, its volatilization and oxidation occur simultaneously at ca. 200 °C [37]. Ciach et al. also report that $SnCl_4$ is eliminated at around 200 °C [38]. Admittedly, such temperatures are higher than those reported here. However, the presence of Pt can play a pivotal role in promoting Sn elimination. In fact, Levy et al. studied the thermal stability of Pt–Sn complexes, concluding that Sn losses occur between 120 and 160 °C [39], a temperature range in line with the results presented in this paper.

In addition, the peak associated with Pt^{4+} to Pt^{2+} reduction in the DTG profile of the PtSn/C samples is less intense than in Pt/C, disappearing in fact in the DTG profile recorded for the Pt_1Sn_3/C sample. This is because Sn^{2+} reduces Pt^{4+} to Pt^{2+}, being itself oxidized to Sn^{4+}. Solutions of Sn^{2+} have slight reducing properties, being used in the synthesis of colloidal Au by reduction of Au^{3+} [40].

3.3. Hydrolytic precipitation of Sn

Considering all the aforementioned results, it is possible to picture the synthesis of Pt_3Sn/C by impregnation. It is well known that Sn^{2+} and Sn^{4+} solutions in water hydrolyze to form Sn hydroxides [41]. Hence, dissolving $SnCl_2$ in water will result in the uncontrolled formation of $Sn(OH)_2$. Furthermore, if $SnCl_2$ is added to a dispersion of carbon in water it will form large particles of $Sn(OH)_2$. In order to achieve a controlled deposition of Sn on carbon, $SnCl_2$ was dissolved in 3 M HCl, added to a water solution of H_2PtCl_6, with the final solution being added to a dispersion carbon in 3 M HCl. In a medium with high [Cl^-], Sn hydrolysis is not favored and $SnCl_2$ tends to form $SnCl_3^-$ and $SnCl_4$ forms $SnCl_6^{2-}$ species. Such tin-chloride species are eliminated during thermal treatment, as shown above, so in order to avoid Sn losses, they should be transformed to Sn oxide or hydroxide species. Chlorides were eliminated by rinsing the samples in water until pH ca. 6.5, and complete Sn hydrolysis was achieved. This process leads to a sharp decrease in the concentration of chloride ions on the samples, while Sn^{2+} and Sn^{4+} cations hydrolyze according to the following equations:

$$Sn^{2+} + H_2O \leftrightarrow Sn(OH)^+ + H^+, \quad \log K = -3.7 \tag{1}$$

$$Sn^{4+} + H_2O \leftrightarrow Sn(OH)_2{}^+ + H^+, \quad \log K = 0.57 \tag{2}$$

Furthermore, Sn hydroxides precipitate as SnO_2 in a pH range from lower than 0 to 14, with the process being favored by thermal treatment in air. In fact, SnO_2 species are clearly observed in the PtSn-*aged* sample. This line of reasoning fits well with the results described for the synthesis of PtSn/C by impregnation. If the PtSn/C samples are subjected to thermal treatments without complete removal of the chloride ions, the final Sn loading of the sample is below the nominal value due to $SnCl_x$ removal during the treatment. However, rinsing the sample until the pH of the recovered water is ≈7 results in the preferential formation of Sn hydroxyl species. SnO_2 is formed after thermal treatment in air. It also explains the presence of SnO_2 in the samples where chloride ions are removed prior to the reducing treatment (see characterization data for the PtSn-*aged* sample). Finally, thermal treatment in hydrogen results in the formation of Pt_3Sn/C.

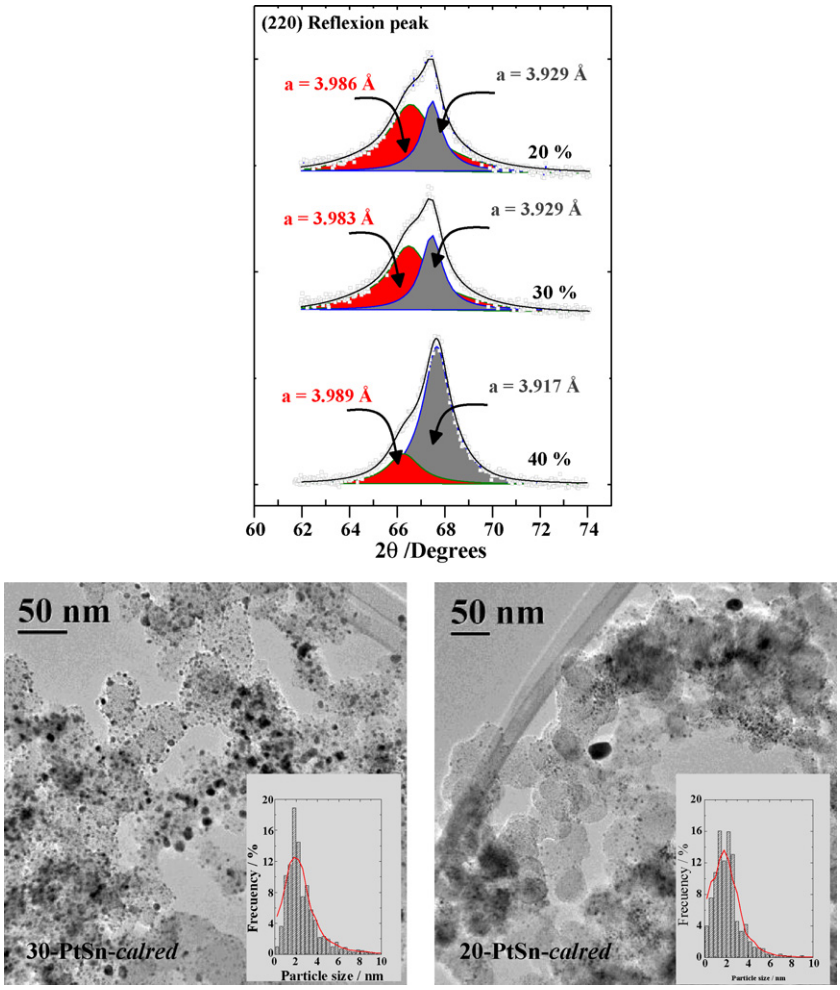

Fig. 7. Diffractogram of the Pt_3Sn/C samples displaying the 2q region corresponding to the (2 2 0) peak. The contribution of two set of Pt fcc peaks is observed. The lattice parameter of each phase is shown in the figure. Below two representative micrographs of 30-PtSn-agedcalred and 20-PtSn-agedcalred are shown, the inset is a histogram of particle size distribution of each electrocatalyst.

To ensure reproducibility of the method, two further electrocatalysts 30-PtSn-*agedcalred* and 20-PtSn-*agedcalred* were prepared starting from the metal salt precursors. The Pt to Sn atomic ratio of those samples derived from EDX analysis is 3, in line with the value found for PtSn-*agedcalred*, see Fig. 3. Fig. 7a shows the 2 2 0 reflection peaks of both catalysts, along with that of PtSn-*agedcalred*. The presence of the Pt_3Sn phase is deduced from the broadening of the peaks to the lower 2θ values. Fig. 7b and c depict representative TEM micrographs of 30-PtSn-*agedcalred* and 20-PtSn-*agedcalred* respectively. The mean particle size of each of those samples, 2.6 ± 1.7 and 2.2 ± 1.8 nm, respectively for the 30 and 20 wt% samples, is slightly smaller than that found for PtSn-*agedcalred* probably due to the higher metal content of latter sample. These results confirm that the impregnation-reduction approach is suitable for preparing carbon-supported Pt_3Sn samples. The preferential formation of the intermetallic phase Pt_3Sn can be achieved by avoiding the elimination of Sn during the rinsing and/or thermal treatments. Such elimination process is in turn favored by the presence of Cl^- ions.

3.4. Electrocatalysts for CO_{ad} and ethanol electrooxidation

The performance of the three Pt_3Sn/C electrocatalysts in the ethanol and CO electrooxidation reactions was studied by means of cyclic voltammetry and CO_{ad} stripping analysis, respectively. Prior to those studies, the samples were subjected to an activation protocol consisting in repeated cycling between 0 and 1 V vs. RHE at 50 mV s^{-1} for 10 cycles.

For the CO_{ad} stripping analysis, the potential was set at 20 mV and CO was admitted in the cell for 15 min. Non-adsorbed CO was then bubbled out of the electrochemical cell by flowing Ar for 45 min. At this stage, three consecutive cycles from 0 to 1 V were recorded at 10 mV s^{-1}. Fig. 8 shows the forward scan of the CO_{ad} oxidation profiles recorded for the PtSn-*agedcalred*, 30-PtSn-*agedcalred*, 20-PtSn-*agedcalred*, PtSn-*calred* and Pt/C samples. CO_{ad} oxidation in PtSn-*agedcalred* starts at around 200 mV, whereas it commences at ca. 600 and 660 mV for PtSn-*calred* and Pt/C, respectively. The shift to less positive potentials is because Sn is more oxophilic than Pt, thereby promoting the formation of OH_{ad} species from water on the Sn sites, that is, to the bifunctional mechanism [7,42]. The CO_{ad} stripping profile recorded for the PtSn-*agedcalred* sample illustrates how CO_{ad} is oxidized over a broad potential window, beginning at potentials of around 200 mV. The CO_{ad} oxidation profile recorded for 30-PtSn-*agedcalred*, 20-PtSn-*agedcalred* is similar to that of PtSn-*agedcalred* only the onset potential of the CO_{ad} oxidation in is shifted by ca. 50 mV to more positive potentials, probably due to the lower amount of metal on such electrodes. Similar performances have been reported previously [5] and reflect the coexistence of Pt_3Sn and Pt-like crystals on the electrocatalysts, in close agreement with our characterization results, see XRD in Fig. 7. On the other hand, being composed mainly of Pt particles, the PtSn-*calred* catalyst records a similar performance to Pt/C.

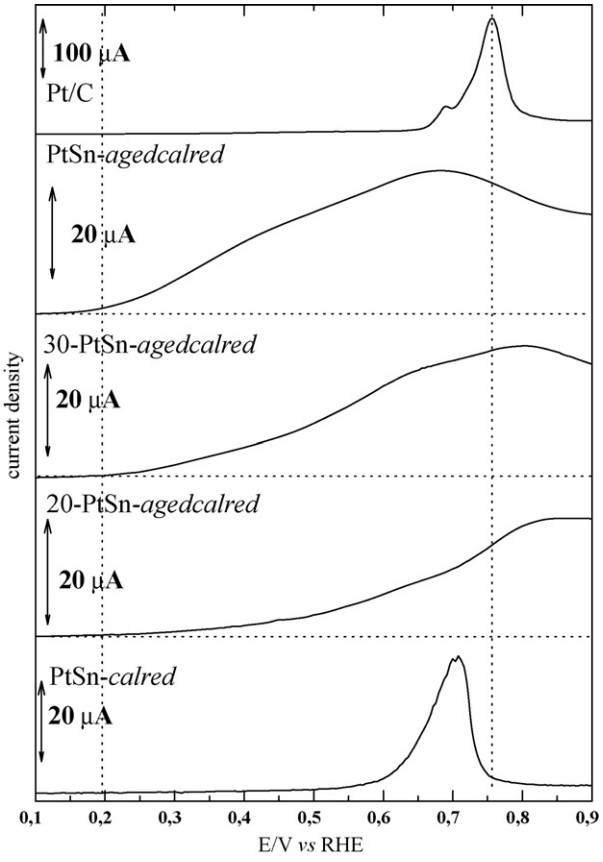

Fig. 8. Comparison of the forward scan of the CO_{ad} stripping analysis recorded in 0.1 M $HClO_4$ at 10 mV s^{-1} for Pt/C, PtSn-*agedcalred*, 30-PtSn-*agedcalred*, 20-PtSn-*agedcalred* and PtSn-*calred*.

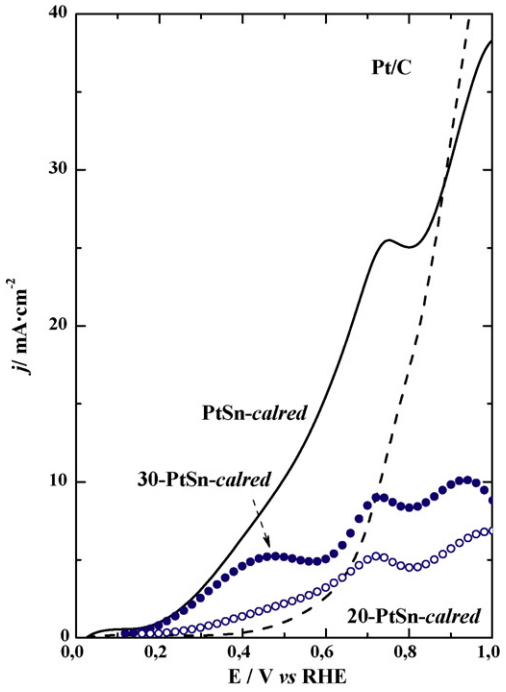

Fig. 9. Comparison of the ethanol electrooxidation *j–E* curves recorded in 0.1 M CH_3CH_2OH + 0.1 M $HClO_4$ at 10 mV s^{-1} for PtSn-*agedcalred* (straight line), 30-PtSn-*agedcalred* (filled circles), 20-PtSn-*agedcalred* (open circles) and commercial Pt/C (dash line) electrodes.

The CO_{ad} oxidation on PtSn-*calred* and Pt/C occurs in a relatively sharp peak centered at 700 and 750 mV, respectively. This marginal promotional effect reflects the presence of a ~3 wt% Sn on that sample (see Table 1). Even if CO_{ad} oxidation is promoted in the Sn-containing samples, particularly in PtSn-*agedcalred*, the adsorbed CO is not fully oxidized until potentials of around 900 mV.

Fig. 9 shows the polarization curves recorded for ethanol electrooxidation on the PtSn-*agedcalred*, 30-PtSn-*agedcalred*, 20-PtSn-*agedcalred* and Pt/C sample. Once again, the performance of the bimetallic samples, particularly those in which the Pt_3Sn phase has been developed, is superior to that of Pt/C and similar to already published studies [6]. The onset potential of the ethanol electrooxidation, deduced from a positive net current value, is observed at ca. 200 mV, which is a significant less positive value than that reported in [43], although it must be pointed out that reaction conditions, such us electrolyte or scan rate are different. In fact, ethanol oxidation in the Pt_3Sn sample is superior to that recorded for Pt/C until potentials of above 750 mV, in other words, those potentials relevant for DAFC applications. The superior tolerance to CO of PtSn-*agedcalred* cannot explain its superior performance, at least at low potentials. As shown in the stripping analysis (Fig. 8), CO_{ad} oxidation in PtSn-*agedcalred* starts only at potentials more positive than 200 mV.

Ethanol adsorbs on Pt sites through a dissociative mechanism [44,45] as depicted in Eqs. (3) and (4):

$$Pt + CH_3–CH_2OH \leftrightarrow Pt–OCH_2–CH_3 + e^- + H^+ \quad (3)$$

$$Pt + CH_3–CH_2OH \leftrightarrow Pt–CHOH–CH_3 + e^- + H^+ \quad (4)$$

This in turn suggests that the oxidation current recorded during ethanol oxidation at low potentials is due to a more facile adsorption/dehydrogenation of ethanol on PtSn/C than on Pt/C. Spectroscopic data also point to this, suggesting that the H_{upd}, which is more strongly bonded on Pt/C, blocks ethanol adsorption sites [12]. Nevertheless, effects such as the downward d-band shift of Pt in Pt_3Sn [46] and the modification of the Pt–Pt interatomic distance by Sn incorporation could play a major role in the ethanol adsorption/oxidation process.

4. Conclusions

The impregnation-reduction approach is a simple route for synthesizing high-loaded, well-dispersed carbon-supported Pt_3Sn nanosized particles. Nevertheless, in order to avoid Sn losses it is necessary to remove chloride ions before subjecting the material to any thermal treatment. This can be achieved by dispersing the electrocatalysts precursors in abundant water and recovering them with a rotary evaporator until the pH of the recovered water is ca. 6.5. In this way, Sn precipitates as hydroxide or oxide species that are stable during thermal treatment. Otherwise, volatile $SnCl_x$ species result in electrocatalysts with a Pt loading that is higher than the nominal value. In the CO and ethanol electrooxidation reaction, the electrocatalysts perform on a par with the catalysts of similar composition and structure prepared by more or less complicated routes.

Acknowledgements

Project ENE2007-67533-C02-01 of the Spanish Ministry of Education and Science is acknowledged for financial support. S. García acknowledges I3P program for a grant.

References

[1] C. Lamy, J.M. Léger, S. Srinivasan, in: J.O.M. Bockris, B.E. Conway, R. White (Eds.), Modern Aspects of Electrochemistry, Kluwer Academic/Plenum Publishers, New York, 2001, pp. 53–118.

[2] F. Vigier, S. Rousseau, C. Coutanceau, J.M. Léger, C. Lamy, Top. Catal. 40 (2006) 111–121.
[3] S. Rojas, F.J. García-García, S. Järas, M.V. Martínez-Huerta, J.L.G. Fierro, M. Boutonnet, Appl. Catal. A 285 (2005) 24–35.
[4] M.V. Martínez-Huerta, J.L. Rodríguez, N. Tsiouvaras, M.A. Peña, J.L.G. Fierro, E. Pastor, Chem. Mater. 20 (2008) 4249–4259.
[5] M. Arenz, V. Stamenkovic, B.B. Blizanac, K.J. Mayrhofer, N.M. Markovic, P.N. Ross, J. Catal. 232 (2005) 402–410.
[6] S. García-Rodríguez, F. Somodi, I. Borbáth, J.L. Margitfalvi, M.A. Peña, J.L.G. Fierro, S. Rojas, Appl. Catal. B 91 (2009) 83–91.
[7] N.M. Markovic, P.N. Ross, CATTECH 4 (2000) 110–126.
[8] V. Radmilovic, T.J. Richardson, S.J. Chen, P.N. Ross Jr., J. Catal. 232 (2005) 199–209.
[9] W. Zhou, Z. Zhou, S. Song, W. Li, G. Sun, P. Tsiakaras, Q. Xin, Appl. Catal. B 46 (2003) 273–285.
[10] V. Stamenkovic, M. Arenz, B.B. Blizanac, K.J.J. Mayrhofer, P.N. Ross, N.M. Markovic, Surf. Sci. 576 (2005) 145–157.
[11] C. Dupont, Y. Jugnet, D. Loffreda, J. Am. Chem. Soc. 128 (2006) 9129–9136.
[12] Q. Wang, G.Q. Sun, L.H. Jiang, Q. Xin, S.G. Sun, Y.X. Jiang, S.P. Chen, Z. Jusys, R.J. Behm, Phys. Chem. Chem. Phys. 9 (2007) 2686–2696.
[13] A. Kowal, S.L. Gojkovic, K.S. Lee, P. Olszewski, Y.E. Sung, Electrochem. Commun. 11 (2009) 724–727.
[14] A. Kowal, M. Li, M. Shao, K. Sasaki, M.B. Vukmirovic, J. Zhang, N.S. Marinkovic, P. Liu, A.I. Frenkel, R.R. Adzic, Nat. Mater. 8 (2009) 325–330.
[15] W.J. Zhou, W.Z. Li, S.Q. Song, Z.H. Zhou, L.H. Jiang, G.Q. Sun, Q. Xin, K. Poulianitis, S. Kontou, P. Tsiakaras, J. Power Sources 131 (2004) 217–223.
[16] A.E. Aksoylu, M.M.A. Freitas, J.L. Figueiredo, Appl. Catal. A 192 (2000) 29–42.
[17] F. Coloma, A. Sepúlveda-Escribano, J.L.G. Fierro, F. Rodríguez-Reinoso, Appl. Catal. A 136 (1996) 231–248.
[18] J. Ribeiro, D.M. Dos Anjos, J.M. Léger, F. Hahn, P. Olivi, A.R. De Andrade, G. Tremiliosi-Filho, K.B. Kokoh, J. Appl. Electrochem. 38 (2008) 653–662.
[19] M.C. Roman-Martinez, J.A. Macia-Agullo, I.M.J. Vilella, D. Cazorla-Amoros, H. Yamashita, J. Phys. Chem. C 111 (2007) 4710–4716.
[20] C. Coutanceau, S. Brimaud, C. Lamy, J.M. Léger, L. Dubau, S. Rousseau, F. Vigier, Electrochim. Acta 53 (2008) 6865–6880.
[21] C. Lamy, S. Rousseau, E.M. Belgsir, C. Coutanceau, J.M. Léger, Electrochim. Acta 49 (2004) 3901–3908.
[22] L. Jiang, Z. Zhou, W. Li, W. Zhou, S. Song, H. Li, G. Sun, Q. Xin, Energy Fuels 18 (2004) 866–871.
[23] A.O. Neto, R.R. Dias, M.M. Tusi, M. Linardi, E.V. Spinacé, J. Power Sources 166 (2007) 87–91.
[24] Z. Liu, B. Guo, L. Hong, T.H. Lim, Electrochem. Commun. 8 (2006) 83–90.
[25] L. Jiang, H. Zang, G. Sun, Q. Xin, Chin. J. Catal. 27 (2006) 15–19.
[26] L. Jiang, G. Sun, S. Sun, J. Liu, S. Tang, H. Li, B. Zhou, Q. Xin, Electrochim. Acta 50 (2005) 5384–5389.
[27] Z. Liu, D. Reed, G. Kwon, M. Shamsuzzoha, D.E. Nikles, J. Phys. Chem. C 111 (2007) 14223–14229.
[28] J. Llorca, P.R. Delapiscina, J.L.G. Fierro, J. Sales, N. Homs, J. Catal. 156 (1995) 139–146.
[29] E.M. Crabb, R. Marshall, D. Thompsett, J. Electrochem. Soc. 147 (2000) 4440–4447.
[30] D.-H. Lim, D.-H. Choi, W.-D. Lee, H.-I. Lee, Appl. Catal. B 89 (2009) 484–493.
[31] F.L.S. Purgato, P. Olivi, J.M. Léger, A.R. de Andrade, G. Tremiliosi-Filho, E.R. Gonzalez, C. Lamy, K.B. Kokoh, J. Electroanal. Chem. 628 (2009) 81–89.
[32] D.L. Boxall, E.A. Kenik, C.M. Lukehart, Chem. Mater. 14 (2002) 1715–1720.
[33] R. Tarozaitė, L. Tamašauskaitė Tamašiūnaitė, V. Jasulaitienė, J. Solid State Electrochem. 13 (2009) 721–731.
[34] F. Colmati, E. Antolini, E.R. Gonzalez, Appl. Catal. B 73 (2007) 106–115.
[35] P.A. Simonov, V.A. Likholobov, in: A. Wieckowski, E.R. Savinova, C.G. Vayenas (Eds.), Catalysis and Electrocatalysis at Nanoparticle Surfaces, Marcel Dekker Inc., New York, 2003, pp. 409–452.
[36] A.E. Schweizer, G.T. Kerr, Inorg. Chem. 17 (1978) 2326–2327.
[37] B. Čerič, P. Bukovec, Thermochim. Acta 195 (1992) 73–84.
[38] S. Ciach, D.J. Knowles, A.J.C. Nicholson, D.L. Swingler, Inorg. Chem. 12 (2002) 1443–1446.
[39] C.J. Levy, R.J. Puddephatt, Organometallics 16 (1997) 4115–4120.
[40] A. Vaskelis, R. Tarozaitė, A. Jagminiene, L.T. Tamasiunaite, R. Juskenas, M. Kurtinaitiene, Electrochim. Acta 53 (2007) 407–416.
[41] C.I. House, G.H. Kelsall, Electrochim. Acta 29 (1984) 1459–1464.
[42] M. Watanabe, S. Motoo, J. Electroanal. Chem. 60 (1975) 275–283.
[43] J.H. Kim, S.M. Choi, S.H. Nam, M.H. Seo, S.H. Choi, W.B. Kim, Appl. Catal. B 82 (2008) 89–102.
[44] F. Vigier, C. Coutanceau, F. Hahn, E.M. Belgsir, C. Lamy, J. Electroanal. Chem. 563 (2004) 81–89.
[45] F. Vigier, C. Coutanceau, A. Perrard, E.M. Belgsir, C. Lamy, J. Appl. Electrochem. 34 (2004) 439–446.
[46] P. Liu, A. Logadottir, J.K. Norskov, Electrochim. Acta 48 (2003) 3731–3742.